



Pipeline of Optimization Techniques for Multi-Level Thresholding in Medical Image Compression Using 2D Histogram

Vimala Kumari Gollu^{1*}, Ganta Usha Sravani², Mandru Sunil Prakash¹, Ganta Srikanth¹

¹ MVGR College of Engineering (A), Vizianagaram 535005, Andhra Pradesh, India

² Publicis Sapient, Bangalore 560037, India

Corresponding Author Email: vimalakumari7@mvgrce.edu.in

<https://doi.org/10.18280/ts.380409>

ABSTRACT

Received: 3 May 2020

Accepted: 12 April 2021

Keywords:

genetic algorithm (GA), image compression, image thresholding, particle swarm optimization (PSO), symbiotic organisms search (SOS), 2-D histogram

In recent times, medical scan images are crucial for accurate diagnosis by medical professionals. Due to the increasing size of the medical images, transfer and storage of images require huge bandwidth and storage space, and hence needs compression. In this paper, multilevel thresholding using 2-D histogram is proposed for compressing the images. In the proposed work, hybridization of optimization techniques viz., Genetic Algorithm (GA), Particle Swarm Optimization (PSO) and Symbiotic Organisms Search (SOS) is used to optimize the multilevel thresholding process by assuming the Renyi entropy as an objective function. Meaningful clusters are possible with optimal threshold values, which lead to better image compression. For performance evaluation, the proposed work has been examined on six Magnetic Resonance (MR) images of brain and compared with individual optimization techniques as well as with 1-D histogram. Recent study reveals that peak signal to noise ratio (PSNR) fail in measuring the visual quality of reconstructed image because of mismatch with the objective mean opinion scores (MOS). So, we incorporate weighted PSNR (WPSNR) and visual PSNR (VPSNR) as performance measuring parameters of the proposed method. Experimental results reveal that hGAPSO-SOS method can be accurately and efficiently used in problem of multilevel thresholding for image compression.

1. INTRODUCTION

Medical images are an efficient source for better diagnosis of the disease and also help in assessing the severity of the disease. Their effective transmission of the diagnosis details through telemedicine benefits rural areas at times of emergencies or doctors' absence or unavailability of the infrastructure. They play a significant part in identifying internal structure of the human body and helps understand the affected areas. But due to their increasing size, transfer and storage requires huge bandwidth and storage space, hence needs compression. Image compression reduces size of the image or video that is to be transmitted by removing irrelevant or repeated bits, so that image can be stored and transmitted in an efficient form and it reduces the Bits per Pixel (BPP), and maintain quality in reconstructed image. In general, images of the medical scan can be compressed in two ways: lossless compression and lossy compression. As the images that are to be provided for physicians and surgeons need to be of high quality and as lossless compression techniques provide low compression ratio it is quite difficult to transmit large amounts of data. In such a condition, lossy compression technique that comes with good compression ratio is needed. Therefore, it is essential to derive effective compression algorithms which have minimal loss, less time complexity, increased reduction in size and still preserve a significant amount of quality in reconstructed image. To achieve this, Various strategies for Image compression are developed and is ordered into two classes,

with and without transform technique. JPEG is the principal global lossy transformed approach and is advantageous for consistent tone still gray scale and color image compression. International Organization for Standardization (ISO) and International Electro-specialized Commission (IEC) together presented JPEG in 1992 [1]. DCT is utilized as transform technique in JPEG image compression. The element of DCT is that the large portion of the energy is focused on D.C coefficients and in low frequency sub-band [2]. After progressive creation of DWT, image compression has been moved to next stage which offers enhanced reformed image quality with high compression [3, 4]. Due to tedious coding measure, the computational complexity of JPEG-2000 is slower than JPEG by 30 times [5, 6].

Quantization is of two types: scalar quantization and vector quantization. When compared to scalar quantization, execution of Vector Quantization (VQ) procedure is superior. VQ is essentially a C-means clustering technique broadly utilized for image compression [7]. Linde et al. presented the Linde-Buzo-Gray (LBG) algorithm, which starts with the lowest codebook size and bit by bit increment size of codebook, utilizing a parting system [8] to progress the enactment of c-means. LBG algorithm is simple, adaptable and flexible but, does not guarantee the best global solutions. Recently, the evolutionary optimization algorithms had been developed to design the codebook for improving the results of LBG algorithm. Rajpoot et al. designed a codebook by using an ant colony system (ACS) algorithm [9]. Moreover, vector quantization using particle swarm optimization (PSO)

[10] beats LBG algorithm, which depends on solution of updating the global best (gbest) and local best (lbest). Wang et al. developed Quantum particle swarm algorithm (QPSO), to tackle the 0–1 backpack issue [11]. Kumari et al. proposed Flower Pollination Algorithm (FPA) for efficient codebook design to compress the medical images [12]. Vector quantization is one which is utilized for clustering the image and data. But due to time consuming procedure, design of codebook is troublesome task [13]. Fractal image compression is a non-transformation technique where image is changed into more modest locales for improved image compression however this procedure is totally tedious [14]. Another non-transformation technique is Artificial Neural Networks, is accomplished for image compression by the neural organization; the outcomes are demonstrated that the training algorithm and the back propagation neural organization can expand the performance [15, 16]. Mardani et al. have used Generative Adversarial Neural Networks (GANs) based compressive sensing framework to model the (low-dimensional) manifold of high-quality MR images [17]. Gözcü et al. have proposed a learning-based framework for optimizing MRI subsampling patterns for a specific reconstruction rule and anatomy [18]. Gao and Xiong have proposed a deep learning framework for the enhancement of compressed brain images [19]. Another non-transformation procedure is thresholding. Thresholding is performed as in otsu technique by class variance or depending on the criterion of entropies like Shannon, Fuzzy, and Kapur [20, 21]. One of inherent thresholding procedure is Birge–Massart, which is utilized for image compression [22]. A weighted membership function is altered by the spatial information of local and global to improve the results of thresholding MR images in conditional spatial FCM [23]. CT images are segmented by SVM using various kernel functions and optimization of sequential minimal using threshold optimization [24–26].

Kumari et al. proposed Hybrid Bacteria Foraging Optimization Algorithm and Particle Swarm Optimization (HBFOA–PSO) algorithm for effective outcomes of thresholding to achieve improved image compression [27]. Ahilan et al. have proposed the use of PSO and its variants Darwinian PSO and Fractional Order DPSO algorithms for multi-level thresholding for image segmentation for lossless compression of medical images [28]. Hoang et al. proposed a new layered image compression framework with encoder-decoder matched semantic segmentation (EDMS) and shows better results when compared to the state-of-the-art semantic-based image codec [29]. A serious problem of first-order thresholding using 1-D histogram is that the spatial correlation between pixels is not considered. Recent investigations show that the outcomes acquired with 2D histogram oriented methodologies are better than those got with 1D histogram [30]. Farnad et al. have shown that hybrid PSO/GA/SOS algorithm (HPG-SOS) dominates other evolutionary algorithms in terms of convergence, execution time and success rate [31]. This work, therefore, proposes the use of Hybrid Genetic Algorithm Particle Swarm Optimization Symbiotic Organisms Search (hGAPSO-SOS) for effective and efficient 2-D histogram based multilevel thresholding for the first time, for image compression. Multilevel thresholding is developed using 2-D histogram by assuming the Renyi entropy as an objective function. Meaningful/useful clusters are possible with optimal threshold values, which lead to better image thresholding and thereby to the objective of image compression. The obtained

results are compared with individual optimization techniques such as Grey Wolf Optimization (GWO), Moth-flame Optimization (MFO), Flower Pollination Optimization (FPO), Particle Swarm Optimization (PSO), Bacteria Foraging Optimization Algorithm (BFOA), and Hybrid Bacteria Foraging Optimization Particle Swarm Optimization (HBFOA-PSO) and, with 1-D histogram. For the performance evaluation of the proposed work, Peak Signal to Noise Ratio (PSNR), Weighted Peak Signal to Noise Ratio (WPSNR), objective function, Visual PSNR (VPSNR), and Compression Ratio (CR) are considered. In every parameter, the performance of proposed hGAPSO-SOS algorithm with 2-D histogram is better than other state of the art algorithms and, with 1-D histogram.

This paper is organized as follows: Section 2 describes the objective function Renyi Entropy. In Section 3, the algorithms GA, PSO and SOS are explained. The proposed approach is explained in Section 4. Finally, results are discussed in Section 5 followed by Conclusion in Section 6.

2. INTRODUCTION TO RENYI ENTROPY

For additive and independent random events, consider ‘ n ’ array discrete probability distributions (pdf) as $(F_1, F_2, F_3 \dots F_n) \in \Delta_n$ where $\Delta_n = \{(F_1, F_2, F_3 \dots F_n), F_i \geq 0, \text{ and } \sum_{i=1}^n F_i = 1\}$ for random variables $(X_1, X_2, X_3, \dots, X_n)$ then Renyi entropy is given as

$$H_\alpha = \frac{1}{1-\alpha} \log_2 \left(\sum_i F_i^\alpha \right) \quad (1)$$

Here ‘ α ’ is higher than zero and, is approaches towards to one, the Renyi entropy turn out to be Shannon entropy. Basically, image is clustered into two, one conveys object data (cluster C_1) and another conveys background (cluster C_2), at that point Renyi entropy is

$$H_\alpha [C_1] = \frac{1}{1-\alpha} \left[\log_2 \left(\sum_{i=0}^L \left(\frac{F(i)}{F(C_1)} \right)^\alpha \right) \right] \quad (2)$$

$$H_\alpha [C_2] = \frac{1}{1-\alpha} \left[\log_2 \left(\sum_{i=t+1}^{L-1} \left(\frac{F(i)}{F(C_2)} \right)^\alpha \right) \right] \quad (3)$$

where, $F(C_1) = \sum_{i=0}^t F(i)$, $F(C_2) = \sum_{i=t+1}^{L-1} F(i)$, Here F_i is the normalized histogram of image and, ‘ L ’ is highest intensity level of gray scale image. With single threshold value ‘ t ’, the Renyi entropy is given as

$$\phi_\alpha(t) = \arg_{\max} \left([H_\alpha [C_1] + H_\alpha [C_2]] \right) \quad (4)$$

2.1 Concept of multi-level thresholding

With ‘ N ’ threshold values, $t=(t_1, t_2, t_3 \dots t_N)$, the image be partitioned into ‘ N ’ clusters $C=(C_1, C_2, C_3 \dots C_N)$. The Renyi entropy for every distinct cluster is characterized as

$$H_\alpha [C_1] = \frac{1}{1-\alpha} \left[\log_2 \left(\sum_{i=0}^{t_1} \left(\frac{F(i)}{F(C_1)} \right)^\alpha \right) \right] \quad (5)$$

$$H_{\alpha}[C_2] = \frac{1}{1-\alpha} \left[\log_2 \left(\sum_{i=t_1+1}^{t_2} \left(\frac{F(i)}{F(C_2)} \right)^{\alpha} \right) \right] \quad (6)$$

$$H_{\alpha}[C_N] = \frac{1}{1-\alpha} \left[\log_2 \left(\sum_{i=t_{N-1}}^{L-1} \left(\frac{F(i)}{F(C_N)} \right)^{\alpha} \right) \right] \quad (7)$$

where, $F(C_1) = \sum_{i=0}^{t_1} F(i)$, $F(C_2) = \sum_{i=t_1+1}^{t_2} F(i)$ and $F(C_N) = \sum_{i=t_{N-1}}^{L-1} F(i)$.

With 'N' thresholds, the overall Renyi entropy or objective function of image is given as

$$\phi_{\alpha}(t) = \arg_{\max} \left(\left[\begin{array}{c} H_{\alpha}[C_1] + H_{\alpha}[C_2] \\ + \dots + H_{\alpha}[C_N] \end{array} \right] \right) \quad (8)$$

Two fake thresholds are presented t_0 and $t_N=L-1$ which have the condition $t_0 < t_1 < \dots < t_{N-1} < t_N$ to make simpler calculations. The optimal thresholds are attained with any soft computing technique by maximizing the Eq. (8).

2.2 Two-dimensional Renyi entropy

Consider $I(m, n)$ is an intensity of image at spatial location (m, n) with size of the image as 'M×N' for gray scale image, and its 1D-histogram is 'h(x)' for $x \in \{1, 2, 3, \dots, L-1\}$, here 'L' is 256 with elements in histogram as G. In literature, 1D-histogram is used for selection of optimal thresholds and are attained by optimizing the objective function i.e. entropy. The 2-D histogram of an image is found by characterizing a local average of nine neighboring pixels, $I(x, y)$, denoted $g(x, y)$ as

$$g(x, y) = \frac{1}{9} \sum_{i=-1}^1 \sum_{j=-1}^1 f(x+i, y+j) \quad (9)$$

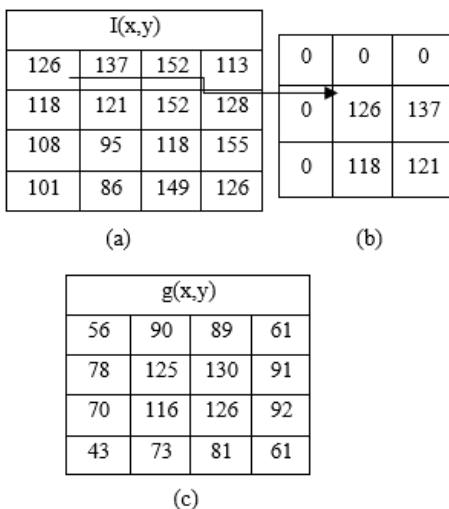


Figure 1. Sample for 2-D histogram calculation

For instance let us take an image of size 4×4 as appeared in Figure 1(a) and its average intensity $g(x, y)$ is determined by padding required number of zeros at edges as appeared in Figure 1(b) for first element i.e. 126 of Figure 1(a), and is given in Figure 1(c).

The 2-D histogram computed using Eq. (9) of the marked area of Metastatic image is shown in Figure 2. It is divided/grouped into four clusters by a single threshold (t, s), where 't' and 's' are thresholds for original image $I(x, y)$ and average image $g(x, y)$ respectively. The area of divided clusters is not the same. From the 2-D histogram, it is seen that corner to corner quadrants convey a lot of data. The diagonal 1st quadrant indicates object, 3rd background and 2nd, 4th quadrants are ignored because they do not convey any information.

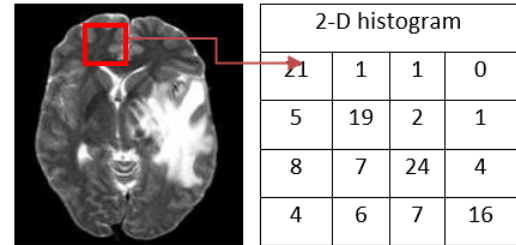


Figure 2. Metastatic image and 2-D histogram

For object and background quadrants, Renyi entropy is given as

$$H_{object}^{\alpha}[t, s] = \frac{1}{1-\alpha} \left[\log_2 \sum_{i=0}^t \left(\sum_{j=0}^s \left(\frac{F(i, j)}{F_{D1}(t, s)} \right)^{\alpha} \right) \right] \quad (10)$$

$$H_{background}^{\alpha}[t, s] = \frac{1}{1-\alpha} \left[\log_2 \sum_{i=t+1}^{L-1} \left(\sum_{j=s+1}^{L-1} \left(\frac{F(i, j)}{F_{D2}(t, s)} \right)^{\alpha} \right) \right] \quad (11)$$

where, $F_{D1}(t, s) = 1 - \sum_{i=0}^t \sum_{j=0}^s F(i, j)$ and, $F_{D2}(t, s) = 1 - \sum_{i=t+1}^{L-1} \sum_{j=s+1}^{L-1} F(i, j)$.

For optimum threshold (t, s) selection, the objective function which is to be maximized is

$$\phi_{\alpha}(t) = \arg_{\max} \left(\left[H_{object}^{\alpha}[t, s] + H_{background}^{\alpha}[t, s] \right] \right) \quad (12)$$

2.3 Multi-level thresholding using 2D-histogram

Thresholding with 2-D histogram conveys superior outcomes particularly in multilevel thresholding. Multilevel thresholding picked up lots of popularity over bi-level thresholding because; it clusters the image into several suitable clusters, helps in precise examination and interpretation of the image [36]. With two thresholds (t_1, t_2) and (s_1, s_2), the 2-D histogram of an image is clustered into 9 clusters as appeared in Figure 3(a). At that point the slanting quadrants first, fifth and ninth represents objects(s) regions, intermediate and background respectively as shown in Figure 3(a) and other regions are noise and edges and are neglected. The 2-D histogram of an image is clustered into 16 clusters with three thresholds (t_1, t_2, t_3) and (s_1, s_2, s_3) as shown in Figure 3 (b).

(0,0)	t ₁	t ₂	(0,L-1)
S ₁	1	2	3
	4	5	6
	7	8	9
(L-1,0)			(L-1,L-1)

(0,0)	t ₁	t ₂	t ₃	(0,L-1)
S ₁	1	2	3	4
	5	6	7	8
	9	10	11	12
S ₂	13	14	15	16
	(L-1,0)			(L-1,L-1)

Figure 3. 2-D histogram: a) 2- level b) 3- level

With two thresholds, Renyi entropy of diagonal quadrants are calculated as

$$H_{object}^{\alpha}[t,s] = \frac{1}{1-\alpha} \left[\log_2 \sum_{i=0}^{t_1} \left(\sum_{j=0}^{s_1} \left(\frac{F(i,j)}{F_{D1}(t,s)} \right)^{\alpha} \right) \right] \quad (13)$$

$$H_{intermediate}^{\alpha}[t,s] = \frac{1}{1-\alpha} \left[\log_2 \sum_{t_1+1}^{t_2} \left(\sum_{s_1+1}^{s_2} \left(\frac{F(i,j)}{F_{D2}(t,s)} \right)^{\alpha} \right) \right] \quad (14)$$

$$H_{background}^{\alpha}[t,s] = \frac{1}{1-\alpha} \left[\log_2 \sum_{t_2+1}^{L-1} \left(\sum_{s_2+1}^{L-1} \left(\frac{F(i,j)}{F_{D3}(t,s)} \right)^{\alpha} \right) \right] \quad (15)$$

where,

$$F_{D1}(t,s) = 1 - \sum_{i=0}^{t_1} \sum_{j=0}^{s_1} F(i,j) \quad , \quad F_{D2}(t,s) = 1 - \sum_{i=t_1+1}^{t_2} \sum_{j=s_1+1}^{s_2} F(i,j) \quad \text{and} \quad F_{D3}(t,s) = 1 - \sum_{i=t_2+1}^{L-1} \sum_{j=s_2+1}^{L-1} F(i,j),$$

for optimum threshold (t, s) selection, the objective function which is to maximize is

$$\varphi_{\alpha}(t) = \arg \max \left(H_{object}^{\alpha}[t,s] + H_{intermediate}^{\alpha}[t,s] + H_{background}^{\alpha}[t,s] \right) \quad (16)$$

For ‘N’ thresholds, the equation is given as

$$\varphi_{\alpha}(t) = \arg \max \left(H_1^{\alpha}[t,s] + H_2^{\alpha}[t,s] + H_3^{\alpha}[t,s] \cdots + H_{N+1}^{\alpha}[t,s] \right) \quad (17)$$

where,

$$H_k^{\alpha}[t,s] = \frac{1}{1-\alpha} \left[\log_2 \sum_{i=t_{k-1}+1}^{t_k} \left(\sum_{j=s_{k-1}+1}^{s_k} \left(\frac{F(i,j)}{F_{DK}(t,s)} \right)^{\alpha} \right) \right] \quad (18)$$

Two dummy variables are selected t_0 and $t_{N+1} = L-1$ which fulfill the condition $t_0 < t_1 < \dots < t_{N-1} < t_N < t_{N+1}$ for simplifying the calculations. Likewise, s_0 and $s_{N+1} = L-1$ are selected with condition $s_0 < s_1 < \dots < s_{N-1} < s_N < s_{N+1}$. The 2-D histogram of four brain MR images is appeared in Figure 4. From the figure, it is seen that the greater part of the data/energy is focused on corner to corner quadrants. Multilevel thresholding is a tedious procedure and is relative to the number of thresholds ‘N’. So, soft computing techniques play a significant role in this challenge by assuming Eq. (17) as an objective function which prompts decrease in the computational time.

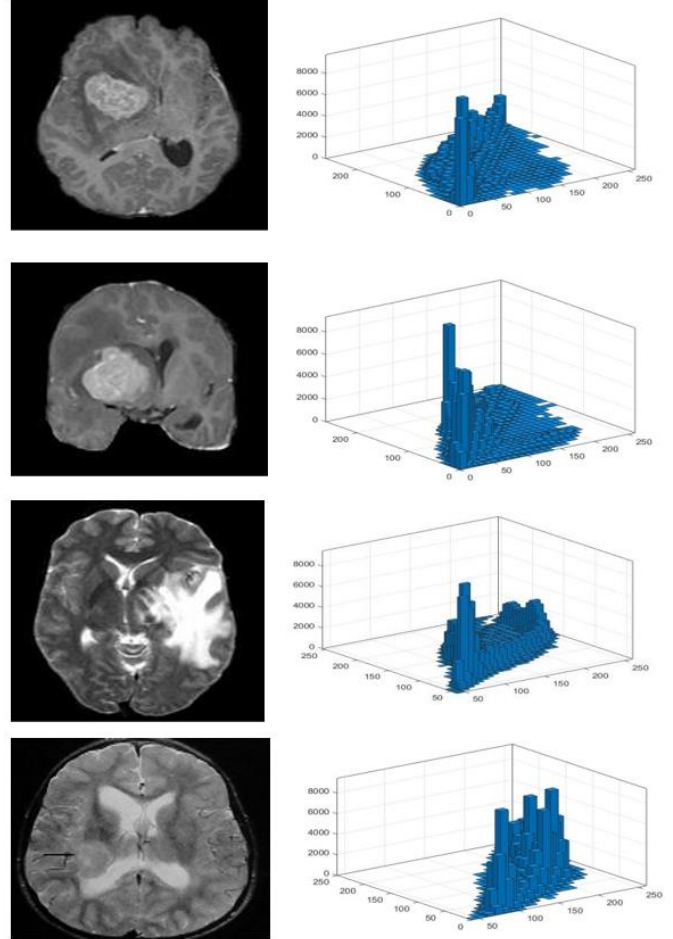


Figure 4. Input images and corresponding 2-D histogram

3. OVERVIEW OF GA, PSO, AND SOS ALGORITHMS

3.1 Genetic Algorithm (GA)

It was initiated and developed between the years 1960s to 1970s by a team called Holland team and is being used for many constrained and unconstrained optimization problems. It is inspired and developed by in-depth study of natural selection of Charles Darwin’s theory [25]. GA being a non-swarm-based technique consists of chromosome for each and every population or solution of the problem. Initial populations are generated by a random number within the range of search space. The ordinary GA uses two steps for selection and creation of new population i.e., mutation operation and crossover operation. The newly generated population or chromosomes are named as offspring. The

crossover operation is performed between two parents for generation of new healthy child. Offspring C is calculated from parents A and B, with the following equation,

$$C_i = \alpha_i A_i + (1 - \alpha) B_i, \quad (19)$$

where, $\alpha_i \in [0,1]$ is a random number.

In all iterations, chromosomes change their values by mutation operation. Mutation in real number is obtained by addition of chromosome with randomly created real number or randomly generated number from Gaussian (normal) distribution. Let A is chromosome and its i^{th} variable is A_i then new offspring A^1 is obtained by mutating i^{th} gene A_i and is calculated with the following equation:

$$A_i^1 = A_i + N, \quad (20)$$

where, 'N' is random number or value taken from Gaussian distribution as

$$N = \text{rand}(0,1)[UB - LB / M],$$

$$LB < A_i \text{ and } A_i^1 < UB$$

Here, 'M' is random real number (range between 1 and 1000, mostly authors prefer M value 10) and $\text{rand}(0,1)$ is a random number lies between 0 to 1. LB and UB are lower limit and upper limit of A_i and A_i^1 respectively.

The genetic algorithm can be explained in the following steps:

- Step 1: Initialize number of chromosomes as N.
- Step 2: Calculate the objective function/fitness function for all N chromosome.
- Step 3: N chromosome are updated by four repeated steps i.e., best chromosome selection – Crossover operation and Mutation operation and finally Replacement.
- Step 4: The generated chromosomes are forwarded for next iterations.
- Step 5: Repeat step 2 - 4 till stopping criteria or maximum Iteration.

3.2 Particle swarm optimization

It is inspired by the searching behavior of particles; some examples are swarm of fish or birds and was developed in the year 1995 by Eberhart and Kennedy 1995 [25]. The PSO, follows randomness and some intelligence in updation of the both particle positions and velocity. The PSO being a swarm-based optimization and is simple and easily adopted for any particle and mathematical problems. Each particle in PSO may be assumed as one bird or one fish and are indicated with O_i . Each particle gains some initial velocity V_i and position O_i of dimensions equal to dimensions of the problem. In all iterations each particle holds some position called personal best (Op) and highest fitness particle holds global best (Obest) position and these positions are updated in upcoming iterations. Let 't' is current iteration, then PSO velocity and position update follows Eq. (21) and Eq. (22).

$$V_{i,d}(t+1) = V_{i,d}(t) + c_1 r_1 (O_{p(i,d)}(t) - O_{i,d}(t)) + c_2 r_2 (O_{best(d)}(t) - O_{i,d}(t)) \quad (21)$$

$$O_{i,d}(t+1) = O_{i,d}(t) + V_{i,d}(t+1) \quad (22)$$

Eq. (21) is for velocity updation and Eq. (22) is for updation of particle position with the help of updated velocities. $Op(i, d)$ is a personal best for particle i and Obest is the best particle among all particle in current iteration 't', c_1 and c_2 are user defined control tuning parameters, r_1 and r_2 are random numbers lying between 0 to 1. The PSO algorithm is as follows.

PSO algorithm:

- 1: Initialize positions of all particles O_i and corresponding velocities V_i .
- 2: Assign highest fitness particle as Obest
- 3: While (termination criterion)
- 4: for $i=1, 2, \dots, n$ do
- 5: Update velocities of all particles by using Eq. (21)
- 6: Update positions of all particles by using Eq. (22)
- 7: Find new objective function of updated particle $O_i(t+1)$
- 8: If new objective function value $O_i(t+1)$ is higher than old $Op, i(t)$ then
- 9: Replace $Op, i(t)$ with $O_i(t+1)$
- 10: end if
- 11: end for
- 12: Now find Obest(t) in all updated particles $Op(t)$
- 13: $itr = itr + 1$ (iteration increment)
- 14: end while
- 15: Finally, outcome Obest is generated.

3.3 Symbiotic organisms search (SOS)

SOS is a soft computing technique developed based on organisms and was proposed in the year 2014 by Prayogo and Cheng, it is inspired by the natural behavior of symbiotic organisms that used to survive in the ecosystem [28]. The fitness for each organism shows the level of adaption to the treated objective. The major advantage of SOS is, it does not require prior tuning of tuning parameters. As like other algorithms, SOS updates the all organism position in each iteration. Position update is done in three successive operations; those are Mutualism, Commensalism and Parasitism. The organism positions will be changed based on best possible relation among all. The algorithm is summarized as following:

1. Initialize the required parameters
2. While (until stopping criterion) do
- Three phases I. Mutualism II. Commensalism III. Parasitism
3. End while

In each iteration, update the phases with the corresponding equations and are as follows.

3.3.1 Mutualism phase

It is a phase, in which both the organisms are benefited, associated with the connection among flowers and honey bees. In this stage, organism O_j randomly selected and it interacts with the other organism O_i . They maintain a good relationship between them so that both organisms get benefited. The updated position of both the organisms is obtained with the following equations.

$$O_{i_{new}} = O_i + \text{rand}(0,1) * (O_{best} - (\text{Mutual_vector} * BF_1)) \quad (23)$$

$$O_{j_{new}} = O_j + rand(0,1) * (O_{best} - (Mutual_vector * BF_2)) \quad (24)$$

$$Mutual_vector = \frac{O_i + O_j}{2} \quad (25)$$

where, *mutal_vector* gives relationship between the organisms O_i and O_j and above equation explains the efforts of mutualistic in gaining their goals and enhance their living survival. The benefit factors BF_1 and BF_2 show how much of benefit organism acquired while interacting with another organism. These two are randomly selected and must be either 1 or 2. O_{best} is the best level of adaption that has established up to this point.

3.3.2 Commensalism phase

This phase is developed on the basis of relation between the Remora fish and sharks. The remora always receives benefits whereas shark may or may not receive benefits from relationship. As discussed in mutualism phase, in this O_i organism gets benefit by maintaining a relationship with randomly selected O_j organism. Then updated equation is (26)

$$O_{i_{new}} = O_i + rand(-1,1) * (O_{best} - O_j) \quad (26)$$

3.3.3 Parasitism phase

This phase exit between the human being and malaria mosquito, in which human being gets effected and some time may die and mosquitoes get benefited with the relationship. As one of the organisms got effected so there is a need to replace with newly generated organism. As like other phases, one organism is selected arbitrarily O_j and it acts as a victim for parasite vector. In problem search space this vector is obtained by duplicating O_i with newly generated and then modifies the randomly chosen organism. If at all this vector is better as compared to O_j then this phase kills O_j and

replace or else O_j gains some energy from parasite and live for some other days.

4. HYBRID ALGORITHM BASED ON GA, PSO AND SOS (HGAPSO-SOS)

Three of the evolutionary algorithms GA, PSO and SOS are combined, represented as hGAPSO-SOS, inspired by Charles Darwin's natural selection for the first time [29]. Here is fact that if any organism has good genetic structure, it leads to a better feature, and has long life in ecosystem. The GA creates a better offspring with good genetic structure from parents. The PSO algorithm gives some important experiences to all organisms which leads better survival of each organism. In the proposed algorithm, PSO follows GA and then SOS follows the sequence.

In all iterations, the hGAPSO-SOS starts with GA with required population, dimension of problem and required initialization of parameters. In next step, all organisms get some best experience with PSO. If any organism position is better as compared to past position, then it will move to better level or else it will remain in same position. If best experience is better than the global best O_{best} , then replace it with new position. So PSO always trying to check for better position by updating the velocity and keep best for the next iterations and also it updates the O_{best} . As all the organisms got some experience with the PSO, now they try to establish a better relation with other organism which leads to better offspring and healthy population. In third phase, if any organism gets improved fitness value, then that organism position is updated with SOS interaction. From the whole observation the GA and SOS are useful for position update and PSO update the O_{best} and personal best of organism. If the current iteration is equal to stopping condition then algorithm stop or else same process is repeated. Block diagram of proposed HGAPSO-SOS algorithm for image compression using multilevel thresholding with 2-D histogram is shown in below Figure 5.

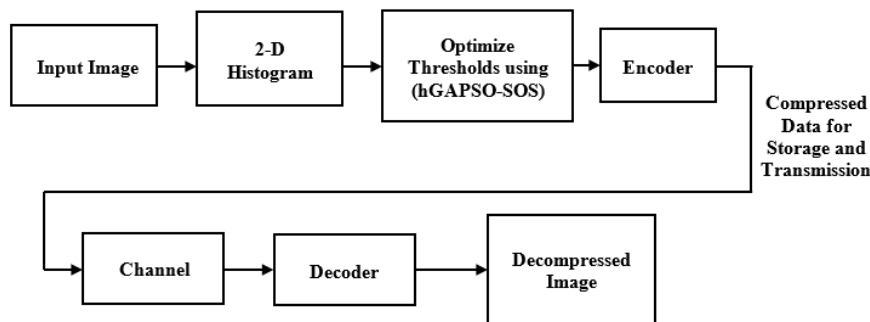


Figure 5. Block diagram of image compression using hGAPSO-SOS Algorithm with 2-D histogram

5. RESULTS AND DISCUSSION

In this paper, Hybridization of GA, PSO, and SOS (HGAPSO-SOS) is used for 2-D histogram by maximizing the Renyi's entropy for effective and efficient image thresholding for image compression. For evaluation of the experiments the method adopted for design of thresholds with the assistance of both 1-D and 2-D histogram is gray scale image coding. Six Magnetic Resonance Imaging (MRI) brain images of four diverse patients with age 3, 32, 35, and

42 taken from BraTS dataset 2018 of size 256×256 namely "Astrocytoma", "Coronary T1 Astrocytoma", "Glioma", "Metastatic", "PNET", and "Meningioma" are adopted for valuation of compression and each pixels take 8 bits (bits per pixel=8). The programs are implemented using Matlab15a with 100 initial solutions. The performance of the proposed hGAPSO-SOS algorithm is compared with six different algorithms namely GWO, MFO, FPO, PSO, BFOA and hBFOA-PSO with thresholds of five.

5.1 Performance metrics for evaluation

To assess the impact of the hGAPSO-SOS algorithm for the subject of multilevel thresholding, we considered Renyi entropy as fitness function with thresholds ‘5’ and are enhanced with the proposed hGAPSO-SOS for successful and effective image compression. Performance of proposed 2-D histogram thresholding technique is validated with performance metrics of fitness function, standard deviation, PSNR, MSE, WPSNR, VPSNR, CR and BPP against six different algorithms such GWO, MFO, FPO, PSO, BFOA and hBFOA-PSO. Fitness function describes how best a solution is appropriate for the given problem. The standard deviation of maximum fitness function is stability measuring parameters of the algorithm.

5.1.1 Peak signal to noise ratio (PSNR)

The fidelity of encoded image is evaluated using the Peak Signal-to-Noise Ratio (PSNR). The PSNR outlines the visual quality of reconstructed image and is expressed in decibels (dB). If the quality of the reproduced image is better, then it demonstrates the higher estimation of PSNR. The definition of PSNR is

$$PSNR = 10 * \log_{10} \left(\frac{255^2}{MSE} \right) \quad (27)$$

From the Eq. (27), it is clear that PSNR value has increased with the decrement in MSE value.

5.1.2 Mean square error (MSE)

MSE measures the degradation of the reformed image as compared to input image and reconstructed image. MSE calculated as

$$MSE = \frac{1}{M \times M} \sum_{i=1}^M \sum_{j=1}^M (X_{ij} - Y_{ij})^2 \quad (28)$$

where, M×M is the size of image, X_{i,j} and Y_{i,j} denotes the value at the location (i,j) of actual and reconstructed images respectively.

5.1.3 Weighted PSNR (WPSNR)

The WPSNR includes human visual system parameters. The WPSNR is obtained by weighting the PSNR by the human visual system (HVS). The WPSNR is given as

$$WPSNR = 10 * \log_{10} \left(\frac{255^2}{NVF \times MSE} \right) \quad (29)$$

Here, NVF is noise visibility function with the standard deviation block of pixels of size (8×8), given as

$$NVF = \text{norm} \left(\frac{1}{1 + \delta_{block}^2} \right) \quad (30)$$

5.1.4 Visual-PSNR (VPSNR)

The visual MSE of n blocks of image is calculated as

$$VMSE_K = \frac{MSE_K}{1 + 0.5 \sqrt{\sigma_x^K \sigma_y^K}} \quad (31)$$

where, K=1, 2, 3.....n, X and Y are input and decompressed images respectively, N is size of the image block. Then MSE of Kth image block is given as

$$MSE_K = \frac{1}{N} \sum_{i=1}^N (X_i^K - Y_i^K)^2$$

And, standard deviation of the block is calculated as follows

$$\sigma_x^K = \sqrt{\frac{1}{N-1} \sum_{i=1}^N (X_i^K - U_i^K)^2} \text{ and } U_i^K = \frac{1}{N} \sum_{i=1}^N X_i^K$$

Then, VPSNR is given as

$$VPSNR = 10 * \log_{10} \left(\frac{255^2}{VMSE} \right) \quad (32)$$

where, $\overline{VMSE} = \frac{1}{N} \sum_{K=1}^N VMSE_K$.

5.1.5 Compression ratio (CR) and Bits per pixel (BPP)

CR is defined as the ratio of original image size to compressed image size and Bits per Pixel is the number of bits required represent compressed image. CR and BPP are calculated using Eq. (33) and Eq. (34) respectively.

$$CR = \frac{\text{Original image size}}{\text{Compressed image size}} \quad (33)$$

$$BPP = \frac{\text{Number of bits}}{\text{Number of pixels}} \quad (34)$$

5.2 Quantitative analysis

The procured result of the hGAPSO-SOS is compared against six different optimization algorithms such GWO, MFO, FPO, PSO, BFOA and hBFOA-PSO for six MRI brain images Astrocytoma, Coronary T1 Astrocytoma, Glioma, Metastatic, PNET, and Meningioma at number of thresholds Th=5. The bits per pixel (bpp) is the ratio of size of compressed image and number of pixels in compressed image. The values of Bits per Pixel (BPP) are variable and are calculated by encoding the thresholded image with cascaded run length and arithmetic coding. To evaluate bpp versus PSNR results, all the pixels in the input image are supplanted with optimal thresholds. If number of thresholds Th=2, at that point 2 bits are sufficient to represent 2 thresholds. So size of compressed image (in terms of bits) is 256×256×2 (since size of input image is 256×256). In this manner, bpp=(256×256×Th)/(256×256×8). Table 1 gives the relation between the number of thresholds (Th) and bpp.

Table 1. Number of thresholds versus bpp

Number of thresholds (Th)	bpp
2	0.25
3	0.375
4	0.50
5	0.625

In order to analyze the performance of proposed algorithm for metrics of fitness function, standard deviation, PSNR,

MSE, WPSNR, VPSNR, CR and BPP, the number of thresholds T_h is chosen as 5. The results are evaluated and compared in Table 2, Table 3, Table 4, and Table 5 for both 1-D and 2-D histogram. Table 2 below shows the quality metrics of fitness function, and standard deviation. PSNR and MSE values attained from the different algorithms are shown in below Table 3. The principal advantage of PSNR is, it is simple to calculate and the drawback is that, it ignores the attributes of human visual system (HVS). So, there is an

essential of different parameters, which gives esteem value to visual quality. Along these lines, Weighted PSNR (WPSNR) and Visual PSNR (VPSNR) are considered for exact quality metrics of proposed technique. Computational time is the total time taken by the algorithm to produce outcome or results and, is measured in seconds. The WPSNR, VPSNR values and, computational time attained from the different algorithms for MRI brain test images are shown in below Table 4.

Table 2. Performance analysis of fitness function & standard deviation of seven algorithms for brain images

Brain Input Images	Optimization Technique	Fitness function		Standard deviation	
		1-D histogram	2-D histogram	1-D histogram	2-D histogram
Meningioma	GWO	16.172	16.9871	0.117654	0.08711
	MFO	16.631	17.1642	3.61E-15	0.0001
	FPO	16.745	17.2092	5.42E-15	3.61E-15
	PSO	16.913	17.2727	0.410305	0.547852
	BFOA	16.922	17.2311	1.45E-14	1.14E-15
	hBFOA-PSO	16.968	17.3589	3.61E-15	2.01E-15
	hGAPSO-SOS	17.745	18.4089	0.241575	0.125874
Glioma	GWO	19.041	19.5462	0.06534	0.04761
	MFO	19.634	19.7893	4.32E-15	2.08E-14
	FPO	19.642	19.8561	0.12408	0.0909
	PSO	19.658	19.9687	0.204440	0.478956
	BFOA	19.824	20.3785	3.61E-15	1.02E-14
	hBFOA-PSO	19.835	20.3738	3.61E-15	2.01E-15
	hGAPSO-SOS	19.947	20.4214	0.369852	0.587945
Coronary T1 Astrocytoma	GWO	16.965	17.5236	0.03465	0.053441
	MFO	17.452	17.8964	0.0075	1.61E-15
	FPO	18.248	18.3783	0.12238	1.81E-15
	PSO	18.268	18.4124	0.341585	0.014785
	BFOA	18.273	18.5245	7.23E-15	5.01E-14
	hBFOA-PSO	18.348	18.7458	3.61E-15	1.45E-14
	hGAPSO-SOS	18.410	18.9589	0.145789	0.258974
Astrocytoma	GWO	17.244	17.4672	0.078797	0.02483
	MFO	17.635	17.8534	3.61E-15	1.81E-15
	FPO	17.724	17.9251	3.61E-15	1.81E-15
	PSO	17.825	18.1245	0.424639	0.569874
	BFOA	18.040	19.2354	3.61E-15	4.25E-15
	hBFOA-PSO	18.091	19.5478	7.23E-15	6.02E-14
	hGAPSO-SOS	18.658	19.6578	0.458965	0.589745
PNET	GWO	15.971	16.3241	0.144739	0.03428
	MFO	16.912	17.4583	3.61E-15	2.37E-15
	FPO	16.987	17.9475	4.42E-15	3.61E-15
	PSO	17.015	18.4732	0.569382	0.0982
	BFOA	17.075	18.5173	1.08E-14	5.42E-15
	hBFOA-PSO	17.086	18.7549	7.23E-15	6.42E-15
	hGAPSO-SOS	17.987	19.5367	5.42E-15	4.98E-15
Metastatic	GWO	19.011	19.6709	0.038206	0.03401
	MFO	19.704	19.9143	1.08E-14	8.03E-15
	FPO	19.709	20.6160	2.41E-15	1.34E-15
	PSO	19.711	20.8521	0.22731	0.12774
	BFOA	19.762	20.9045	0.0909	9.03E-15
	hBFOA-PSO	19.765	21.0152	0.09090	1.81E-15
	hGAPSO-SOS	19.983	21.2475	0.104217	0.029367

The values of BPP and CR are variable and are calculated by encoding the thresholded image with cascaded run length and arithmetic coding and are given in below Table 5. From the results, it is found that the proposed hybrid algorithm hGAPSO-SOS outperforms in all performance parameters when compared to other algorithms i.e. higher PSNR, lower MSE, better fitness function, and standard deviation and, also noted that the results are better with 2-D histogram when compared with the 1-D histogram. From Table 2, quality metrics such as fitness function and standard deviation were evaluated using proposed hybrid algorithm hGAPSO-SOS on

six MRI brain images and compared with six different algorithms namely GWO, MFO, FPO, PSO, BFOA and hBFOA-PSO, for both 1-D and 2-D histogram at number of thresholds $T_h=5$.

From the table, it is observed that, proposed hGAPSO-SOS technique provides fitness value is 4.7573% more with 1-D, 6.486% more with 2-D than other existing algorithms. From comparison, it is also observed that fitness value provided is 2.514% more with 2-D than 1-D histogram. Figures 6 and Figure 7 below shows the graphical representation of variation in PSNR values of six MRI brain

images Astrocytoma, Coronary T1, Glioma, Metastatic, PNET, and Meningioma of all optimization algorithms obtained with 1-D and 2-D histogram respectively at 0.625 bpp at number of thresholds $Th=5$. The graphical representation of variation in MSE values of six MRI brain images of all optimization algorithms obtained with 1-D and 2-D histogram at 0.625 bpp are shown in below Figure 8 and Figure 9 respectively.

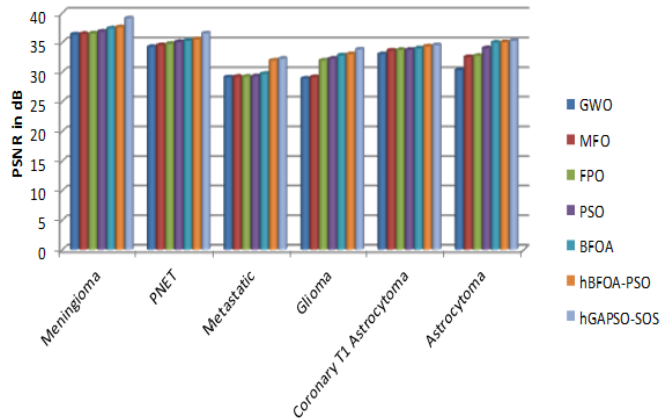


Figure 6. Variation of PSNR obtained with 1-D histogram of MRI brain images at $bpp=0.625$

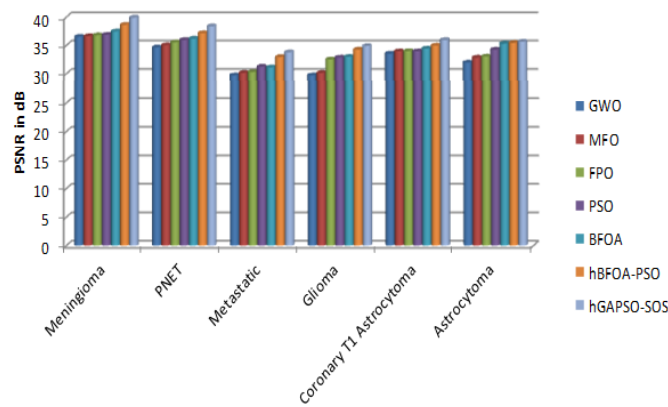


Figure 7. Variation of PSNR obtained with 2-D histogram of MRI brain images at $bpp=0.625$

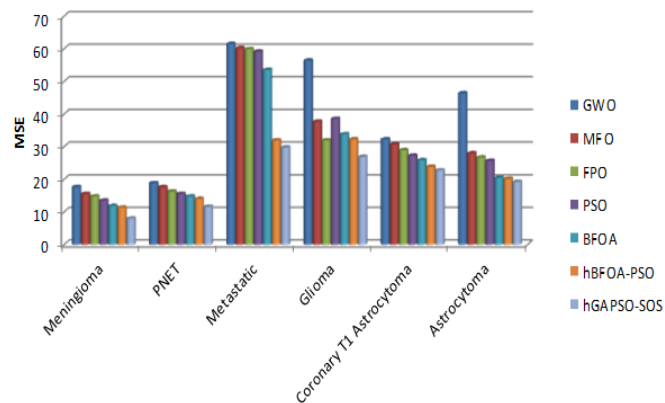


Figure 8. Variation of MSE obtained with 1-D histogram of MRI brain images at $bpp=0.625$

From below Table 3, quality metrics such as PSNR and MSE were evaluated using proposed hybrid algorithm hgAPSO-SOS on six MRI brain images and compared with other six different algorithms for both 1-D and 2-D histogram

at number of thresholds $Th=5$. From the table, it is observed that, proposed hgAPSO-SOS technique provides PSNR is 4.91% more with 1-D, and 4.1% more with 2-D than other existing algorithms. From comparison, it is also observed that PSNR provided is 0.857% more with 2-D than 1-D histogram. From the table, it is clear that proposed hybridization technique provides MSE is 52% less with 1-D, and 49% less with 2-D than other existing algorithms. From comparison, it is also observed that MSE value is 6.7395% less with 2-D than 1-D histogram.

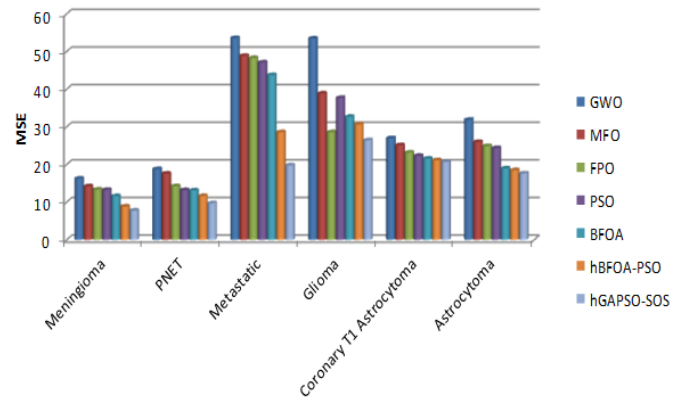


Figure 9. Variation of MSE obtained with 2-D histogram of MRI brain images at $bpp=0.625$

From below Table 4, quality metrics such as WPSNR, VPSNR and Computational time were evaluated using proposed hybrid algorithm hgAPSO-SOS on six MRI brain images and compared with six different algorithms namely GWO, MFO, FPO, PSO, BFOA and hbFOA-PSO, for both 1-D and 2-D histogram at number of thresholds $Th=5$. From the table, it is observed that, proposed hgAPSO-SOS technique provides WPSNR is 5.77% more with 1-D, VPSNR is 18.4787% more with 1-D, 7.69% more WPSNR with 2-D, and 19.16% more VPSNR with 2-D than other existing algorithms. From comparison, it is also observed that WPSNR provided is 4.1575% more with 2-D than 1-D, and 2.23697% more VPSNR with 2-D than 1-D histogram. From the table, it is clear that proposed hybridization technique computational time is little bit higher as compared with other algorithms in 2-D because of cascading GA, PSO, and SOS, and is illustrated in Table 4. But in comparison with the 1-D, computational time is 2.514% lower with 2-D. From the results, it is found that the proposed hybrid algorithm hgAPSO-SOS outperforms in all performance parameters when compared to other algorithms i.e. higher WPSNR, VPSNR, and also noted that, the results are better with 2-D histogram when compared with the 1-D histogram. From comparison of results, it is observed that, proposed hgAPSO-SOS technique gives better compression ratio, i.e. 16.365% using 1-D and, 36.94% using 2-D histogram than the existing techniques GWO, MFO, FPO, PSO, BFOA and hbFOA-PSO, and is illustrated in below Table 5. From the table, it is clear that proposed hybridization technique provides higher compression ratio 68.77% using 2D than 1D histogram. From the results, it is found that the proposed hybrid algorithm hgAPSO-SOS provides better CR than the existing techniques GWO, MFO, FPO, PSO, BFOA and hbFOA-PSO. So, hgAPSO-SOS method can be accurately and capably used in problem of multilevel thresholding using 2-D for image compression.

5.3 Qualitative analysis

Here we focus on visual clarity of decompressed images with the proposed work by maximizing the Renyi entropy by thresholding the image with proposed hybrid GAPSO-SOS and with GWO, MFO, FPO, PSO, BFOA and hBFOA-PSO

algorithms. Figure 10 to Figure 15 below, shows original MRI brain images and the corresponding decompressed images of GWO, MFO, FPO, PSO, BFOA, hBFOA-PSO and hybrid GAPSO-SOS algorithms of Astrocytoma, Coronary T1 Astrocytoma, Glioma, Metastatic, PNET, and Meningioma brain MRI images respectively.

Table 3. Performance evaluation of PSNR & MSE values of seven algorithms for brain images

Brain Input Images	Optimization Technique	PSNR in dB		MSE	
		1-D histogram	2-D histogram	1-D histogram	2-D histogram
Meningioma	GWO	36.36813	36.54231	17.6145	16.3126
	MFO	36.46615	36.64134	15.5373	14.2353
	FPO	36.54133	36.79182	14.7675	13.3815
	PSO	36.84133	36.88658	13.4569	13.31749
	BFOA	37.39621	37.47584	11.8429	11.62777
	hBFOA-PSO	37.58954	38.65026	11.3273	8.872671
	hGAPSO-SOS	39.10687	39.91545	7.9871	7.789962
PNET	GWO	34.26407	34.66402	18.8179	18.8179
	MFO	34.55097	35.05037	17.6144	17.6144
	FPO	34.78454	35.53424	16.2546	14.2641
	PSO	35.09575	35.99365	15.5373	13.2343
	BFOA	35.31654	36.21428	14.7672	13.1532
	hBFOA-PSO	35.55442	37.16502	13.9807	11.6745
	hGAPSO-SOS	36.54231	38.38712	11.5923	9.7609
Metastatic	GWO	29.12323	29.72544	61.4678	53.6106
	MFO	29.21606	30.16525	60.1674	48.8914
	FPO	29.23780	30.29682	59.8663	48.2973
	PSO	29.29132	31.26530	59.1335	47.1272
	BFOA	29.72694	31.15134	53.4896	43.7657
	hBFOA-PSO	31.96948	32.95464	31.9162	28.6059
	hGAPSO-SOS	32.27554	33.79839	29.7458	19.8202
Glioma	GWO	28.92734	29.72694	56.3952	53.489
	MFO	29.18506	30.16053	37.6738	38.891
	FPO	31.96948	32.52526	31.9169	28.605
	PSO	32.27554	32.86587	38.50582	37.7132
	BFOA	32.84134	32.98745	33.80231	32.68401
	hBFOA-PSO	33.04264	34.25874	32.27129	30.70481
	hGAPSO-SOS	33.83699	34.90258	26.87704	26.47417
Coronary T1Astrocytoma	GWO	33.04206	33.5691	32.24120	27.02921
	MFO	33.66409	33.9583	30.71342	25.16091
	FPO	33.75482	33.9987	28.90347	23.18384
	PSO	33.77889	33.96724	27.23901	22.3451
	BFOA	34.00706	34.43670	25.84487	21.6054
	hBFOA-PSO	34.35888	34.97895	23.83375	21.1582
	hGAPSO-SOS	34.56214	35.96587	22.74397	20.72494
Astrocytoma	GWO	30.34729	31.969481	46.369	31.916
	MFO	32.54134	32.855644	27.978	26.025
	FPO	32.74866	33.042064	26.675	24.932
	PSO	34.03859	34.25874	25.65791	24.38969
	BFOA	35.00920	35.33568	20.5192	19.03322
	hBFOA-PSO	35.08465	35.45789	20.1658	18.5051
	hGAPSO-SOS	35.29112	35.65894	19.22952	17.66796

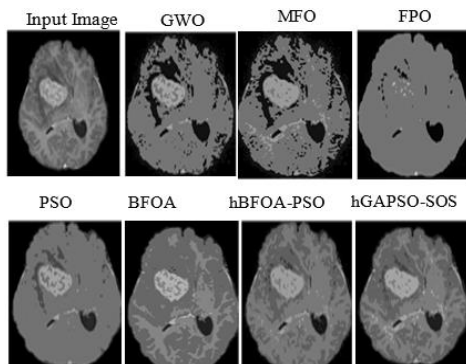


Figure 10. Decompressed images obtained with seven algorithms of Astrocytoma brain image

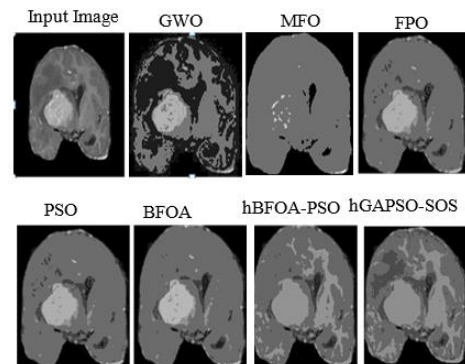


Figure 11. Decompressed images obtained with seven algorithms of Coronary T1 Astrocytoma brain image

Table 4. Comparison of WPSNR, VPSNR and Elapsed time values of brain images for various algorithms

Brain Input Images	Optimization Technique	WPSNR in dB		VPSNR in dB		Elapsed time (sec)	
		1-D	2-D	1-D	2-D	1-D	2-D
		histogram	histogram	histogram	histogram	histogram	histogram
Meningioma	GWO	15.6090	15.847	15.079	15.278	10.781	9.284
	MFO	15.8353	16.189	15.134	15.375	7.238	6.013
	FPO	15.9374	16.492	15.198	15.483	12.435	11.364
	PSO	16.0525	16.768	15.256	15.568	9.224	7.782
	BFOA	18.1255	18.978	16.124	16.258	7.020	5.567
	hBFOA-PSO	19.0003	20.024	17.102	17.478	57.999	49.24
	hGAPSO-SOS	19.7084	20.147	19.258	19.985	64.345	54.421
PNET	GWO	18.1534	18.345	15.264	15.583	16.912	14.957
	MFO	18.5318	18.675	15.459	15.954	7.173	6.023
	FPO	18.7523	18.967	15.973	16.367	17.234	15.024
	PSO	18.9432	19.198	16.247	16.756	9.805	7.643
	BFOA	19.0816	19.543	16.725	17.034	7.602	6.104
	hBFOA-PSO	20.2464	20.349	17.246	17.746	59.418	45.375
	hGAPSO-SOS	20.7398	20.986	18.027	18.958	71.348	58.426
Metastatic	GWO	25.6666	25.813	16.323	16.575	15.427	13.765
	MFO	25.7612	25.985	16.785	16.983	10.716	8.342
	FPO	25.9765	26.078	17.253	17.859	14.274	12.869
	PSO	26.4718	26.654	17.648	18.023	8.235	6.234
	BFOA	26.4960	26.942	17.904	18.867	9.443	7.569
	hBFOA-PSO	26.5009	26.875	18.127	18.849	48.395	36.235
	hGAPSO-SOS	26.7258	27.362	18.984	19.694	59.142	43.654
Glioma	GWO	16.9745	17.324	14.042	14.234	12.145	11.570
	MFO	17.6191	17.976	14.197	14.769	7.867	5.635
	FPO	18.2012	18.574	14.326	15.168	15.562	13.794
	PSO	18.7953	18.987	14.457	16.909	9.9885	6.270
	BFOA	18.9130	18.978	14.698	18.024	17.692	12.781
	hBFOA-PSO	19.1240	19.057	16.457	18.245	52.848	46.251
	hGAPSO-SOS	19.2351	19.333	19.985	19.658	71.753	63.231
Coronary T1 Astrocytoma	GWO	17.6281	17.874	15.109	15.367	16.924	14.768
	MFO	17.8520	17.924	15.298	15.896	9.041	7.325
	FPO	17.905	18.016	15.567	16.638	15.835	13.573
	PSO	18.1561	18.245	16.102	18.214	10.561	7.529
	BFOA	19.9524	19.447	16.247	19.247	8.3687	5.321
	hBFOA-PSO	20.5253	20.727	16.367	22.124	58.186	51.982
	hGAPSO-SOS	20.8112	20.963	18.247	22.247	74.386	64.342
Astrocytoma	GWO	17.0790	17.354	16.018	16.675	21.726	20.047
	MFO	17.6321	17.860	16.249	17.028	8.054	6.958
	FPO	18.7072	18.864	16.573	17.893	16.392	14.538
	PSO	18.8089	18.947	16.957	18.608	13.634	9.527
	BFOA	19.5862	19.658	17.547	18.425	7.9109	4.632
	hBFOA-PSO	19.8229	19.919	18.654	19.962	65.194	56.036
	hGAPSO-SOS	20.1235	20.207	19.102	20.753	83.561	74.375

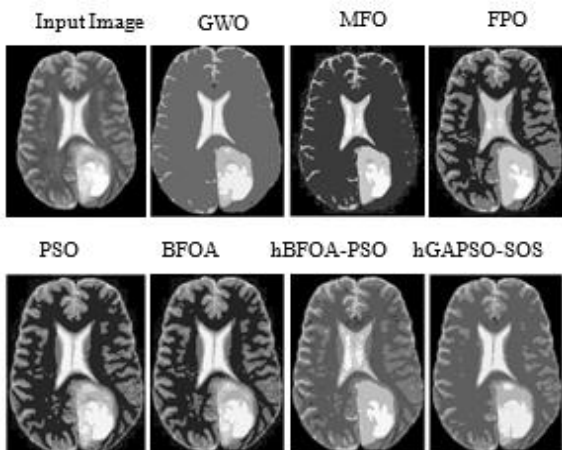


Figure 12. Decompressed images obtained with seven algorithms of Glioma brain image

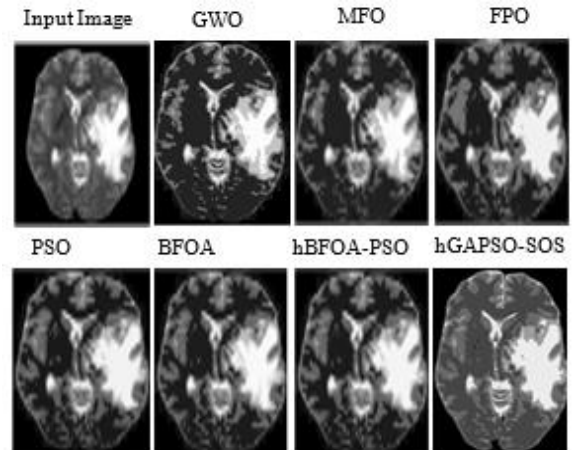


Figure 13. Decompressed images obtained with seven algorithms of Metastatic brain image

Table 5. Evaluation of BPP and CR of seven algorithms for brain images

Image	Optimization Technique	BPPcode		CRcode	
		1-D	2-D	1-D	2-D
Meningioma	GWO	0.2787556	0.5971753	28.69898	13.396401
	MFO	0.2686425	0.5900642	29.779412	13.557847
	FPO	0.3159341	0.5950264	25.323712	13.443581
	PSO	0.3038815	0.7379753	26.326053	10.840471
	BFOA	0.2710123	0.6313086	29.51895	12.67209
	HBFOA-PSO	0.2785975	0.6992593	28.715258	11.440678
	hGAPSO-SOS	0.2644136	0.5981274	30.252436	13.371352
PNET	GWO	0.4979358	0.8427457	16.066328	8.4024896
	MFO	0.5513481	0.895842	14.509888	8.9301464
	FPO	0.5596457	0.8709453	14.296814	9.1857568
	PSO	0.4998321	0.9520988	16.005375	9.1150522
	BFOA	0.537758	0.8776691	14.876579	9.4927808
	HBFOA-PSO	0.4984099	0.7341827	16.051046	10.896478
	hGAPSO-SOS	0.4331901	0.6019214	18.474372	13.292636
Metastatic	GWO	0.6842469	0.9438815	11.691686	8.4756404
	MFO	0.7204346	0.9636346	11.104409	8.3019023
	FPO	0.6060241	0.872634	13.198095	9.1673452
	PSO	0.6844049	0.8918914	11.688986	8.9697023
	BFOA	0.6902519	0.9440395	11.589973	8.4742216
	HBFOA-PSO	0.8124049	0.8564938	9.847306	9.3404059
	hGAPSO-SOS	0.8557365	0.8907356	9.3482158	8.9816747
Glioma	GWO	0.691358	0.8351605	11.571429	9.5789972
	MFO	0.7659457	0.9770667	10.444605	8.1877729
	FPO	0.5596234	0.8557345	14.293127	9.3482134
	PSO	0.5627259	0.857916	14.216512	9.3249217
	BFOA	0.7651556	1.0140444	10.45539	7.8892006
	HBFOA-PSO	0.5619358	0.9034272	14.236502	8.8551688
	hGAPSO-SOS	0.5596236	0.8842670	14.293267	9.0465673
Coronary T1 Astrocytoma	GWO	0.5456593	0.5652543	14.661164	14.152921
	MFO	0.5864296	0.5508741	13.641876	14.522375
	FPO	0.4295543	0.5950232	18.626792	13.442674
	PSO	0.3318519	0.6363654	24.107143	12.571393
	BFOA	0.5897481	0.5357037	13.565113	14.933628
	HBFOA-PSO	0.5347556	0.7085827	14.960106	11.290143
	hGAPSO-SOS	0.5981890	0.5972342	13.375672	13.395672
Astrocytoma	GWO	0.5684148	0.7841185	14.074229	10.202539
	MFO	0.5420247	0.8209383	14.759475	9.7449471
	FPO	0.4295123	0.8624356	18.626793	9.2763452
	PSO	0.3373827	0.8267852	23.711944	9.6760321
	BFOA	0.5564049	0.5782123	14.378018	13.835747
	HBFOA-PSO	0.557037	0.5515062	14.361702	14.505731
	hGAPSO-SOS	0.611978	0.6018234	13.074367	13.294563

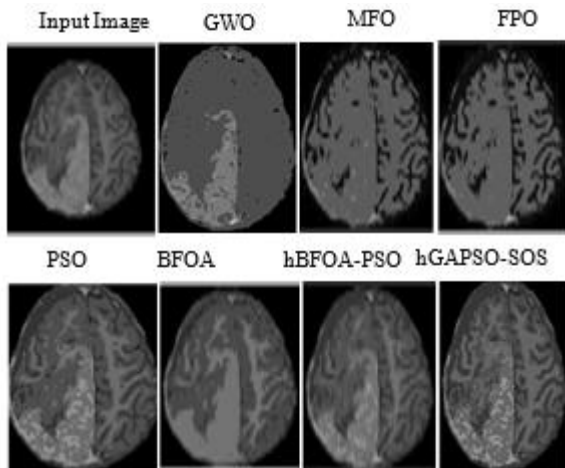


Figure 14. Decompressed images obtained with seven algorithms of PNET brain image

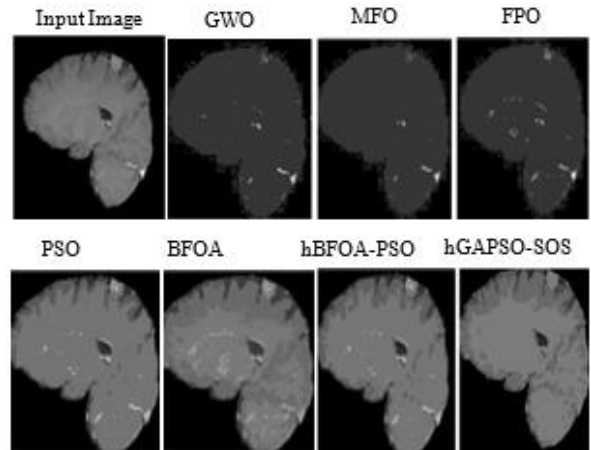


Figure 15. Decompressed images obtained with seven algorithms of Meningioma brain image

From figures, it is seen that decompressed image quality of the proposed hGAPSO-SOS is better than the other individual algorithms.

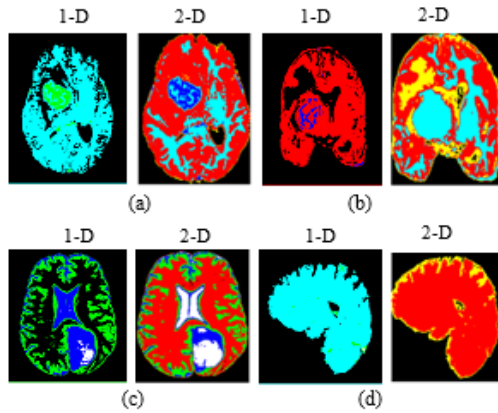


Figure 16. Decompressed images of hGAPSO-SOS algorithm with 1-D and 2-D histogram: (a) Astrocytoma (b) Coronary (c) Glioma (d) Meningioma

For efficiency measure of proposed algorithm hybrid GAPSO-SOS, the visual quality of reconstructed images has to be evaluated in Figure 16 a-d with Renyi entropy at five number of thresholds in 1-D and proposed 2-D histogram. From the figures, it is seen that hGAPSO-SOS visual quality is better for 2-D histogram as related to 1-D histogram.

6. CONCLUSIONS

In this paper, Hybridization of Genetic Algorithm, Particle Swarm Optimization and Symbiotic Organisms Search is used for decisive and efficient multilevel thresholding for image compression. Optimal threshold values are provided by maximizing the Renyi entropy using 2-D histogram which leads to better image thresholding. So, meaningful/useful clusters are possible with optimal threshold values, leads to better image compression. For performance evaluation, the proposed hGAPSO-SOS algorithm is tested on six MR brain images. Performance of proposed 2-D histogram thresholding technique is validated with performance metrics of fitness function, MSE, PSNR, CR, WPSNR, and, VPSNR. The procured result of the hGAPSO-SOS is compared with other optimization algorithms such as GWO, MFO, FPO, PSO, BFOA and hBFOA-PSO. From comparison, it is observed that hGAPSO-SOS algorithm provides better fitness value, higher PSNR, VPSNR, WPSNR values and maintain good quality of the reconstructed images with better CR than other six algorithms. From the results, it is concluded that the Hybridization of optimization algorithms enhances all performance parameters than other individual algorithms and also found to be better with 2-D than with the 1-D histogram. From results, it shows that proposed hGAPSO-SOS method is more reliable than GWO, MFO, FPO, PSO, BFOA and hBFOA-PSO and, can be efficiently used in problem of multilevel thresholding for medical image compression.

REFERENCES

[1] Pennebaker, W.B., Mitchell, J.L. (1992). JPEG: Still Image Data Compression Standard. Springer Science &

Business Media.
 [2] Ahmed, N., Natarajan, T., Rao, K.R. (1974). Discrete cosine transform. *IEEE Transactions on Computers*, 100(1): 90-93. <https://doi.org/10.1109/T-C.1974.223784>
 [3] DeVore, R.A., Jawerth, B., Lucier, B.J. (1992). Image compression through wavelet transform coding. *IEEE Transactions on Information Theory*, 38(2): 719-746. <https://doi.org/10.1109/18.119733>
 [4] Acharya, T., Tsai, P.S. (2005). JPEG2000 Standard for Image Compression: Concepts, Algorithms and VLSI Architectures. John Wiley & Sons. <https://doi.org/10.1002/0471653748.ch6>
 [5] Skodras, A.N., Christopoulos, C.A., Ebrahimi, T. (2001). JPEG2000: The upcoming still image compression standard. *Pattern Recognition Letters*, 22(12): 1337-1345. [https://doi.org/10.1016/S0167-8655\(01\)00079-4](https://doi.org/10.1016/S0167-8655(01)00079-4)
 [6] Santa-Cruz, D., Ebrahimi, T. (2000). An analytical study of JPEG 2000 functionalities. In *Proceedings 2000 International Conference on Image Processing (Cat. No. 00CH37101)*, 2: 49-52. <https://doi.org/10.1109/ICIP.2000.899222>
 [7] De, A., Guo, C. (2015). An adaptive vector quantization approach for image segmentation based on SOM network. *Neurocomputing*, 149: 48-58. <https://doi.org/10.1016/j.neucom.2014.02.069>
 [8] Linde, Y., Buzo, A., Gray, R. (1980). An algorithm for vector quantizer design. *IEEE Transactions on Communications*, 28(1): 84-95. <https://doi.org/10.1109/TCOM.1980.1094577>
 [9] Rajpoot, N.M., Hussain, A., Ali, U., Saleem, K., Qureshi, M. (2004). A novel image coding algorithm using ant colony system vector quantization. In: *International Workshop on Systems, Signals and Image Processing (IWSSIP 2004)*, Poznan, Poland, pp. 13-15.
 [10] Kumar, M., Kapoor, R., Goel, T. (2010). Vector quantization based on self-adaptive particle swarm optimization. *International Journal of Nonlinear Sciences*, 9(3): 311-319.
 [11] Wang, Y., Feng, X.Y., Huang, Y.X., Pu, D.B., Zhou, W.G., Liang, Y.C., Zhou, C.G. (2007). A novel quantum swarm evolutionary algorithm and its applications. *Neurocomputing*, 70(4-6): 633-640. <https://doi.org/10.1016/j.neucom.2006.10.001>
 [12] Kumari, G.V., Rao, G.S., Rao, B.P. (2021). Flower pollination-based K-means algorithm for medical image compression. *International Journal of Advanced Intelligence Paradigms*, 18(2): 171-192. <https://doi.org/10.1504/IJAIP.2021.112903>
 [13] Chiranjeevi, K., Jena, U. (2017). Hybrid gravitational search and pattern search-based image thresholding by optimising Shannon and fuzzy entropy for image compression. *International Journal of Image and Data Fusion*, 8(3): 236-269. <https://doi.org/10.1080/19479832.2017.1338760>
 [14] Sheeba, K., Rahiman, M.A. (2019). Gradient based fractal image compression using Cayley table. *Measurement*, 140: 126-132. <https://doi.org/10.1016/j.measurement.2019.02.038>
 [15] Patel, B., Agrawal, S. (2013). Image compression techniques using artificial neural network. *International Journal of Advanced Research in Computer Engineering & Technology*, 2(10): 2725-2729.
 [16] Kumari, G.V., Rao, G.S., Rao, B.P. (2019). New

- artificial neural network models for bio medical image compression: bio medical image compression. *International Journal of Applied Metaheuristic Computing (IJAMC)*, 10(4): 91-111. <https://doi.org/10.4018/IJAMC.2019100106>
- [17] Mardani, M., Gong, E., Cheng, J.Y., Vasanaawala, S.S., Zaharchuk, G., Xing, L., Pauly, J.M. (2018). Deep generative adversarial neural networks for compressive sensing MRI. *IEEE Transactions on Medical Imaging*, 38(1): 167-179. <https://doi.org/10.1109/TMI.2018.2858752>
- [18] Gözcü, B., Mahabadi, R.K., Li, Y.H., Ilıcak, E., Cukur, T., Scarlett, J., Cevher, V. (2018). Learning-based compressive MRI. *IEEE Transactions on Medical Imaging*, 37(6): 1394-1406. <https://doi.org/10.1109/TMI.2018.2832540>
- [19] Gao, S., Xiong, Z. (2019). Deep enhancement for 3D HDR brain image compression. In 2019 IEEE International Conference on Image Processing (ICIP), pp. 714-718. <https://doi.org/10.1109/ICIP.2019.8803781>
- [20] De Luca, A., Termini, S. (1972). A definition of a nonprobabilistic entropy in the setting of fuzzy sets theory. *Information and Control*, 20(4): 301-312. [https://doi.org/10.1016/S0019-9958\(72\)90199-4](https://doi.org/10.1016/S0019-9958(72)90199-4)
- [21] Tryon, R.C. (2016). Cluster analysis: correlation profile and ortho-metric (factor) analysis for the isolation of unities in mind and personality. *Applied Mathematics*, 7(15): 231-239.
- [22] Sidhik, S. (2015). Comparative study of Birge–Massart strategy and unimodal thresholding for image compression using wavelet transform. *Optik*, 126(24): 5952-5955. <https://doi.org/10.1016/j.ijleo.2015.08.127>
- [23] Adhikari, S.K., Sing, J.K., Basu, D.K., Nasipuri, M. (2015). Conditional spatial fuzzy C-means clustering algorithm for segmentation of MRI images. *Applied Soft Computing*, 34: 758-769. <https://doi.org/10.1016/j.asoc.2015.05.038>
- [24] Ramakrishnan, T., Sankaragomathi, B. (2017). A professional estimate on the computed tomography brain tumor images using SVM-SMO for classification and MRG-GWO for segmentation. *Pattern Recognition Letters*, 94: 163-171. <https://doi.org/10.1016/j.patrec.2017.03.026>
- [25] Salleh, M.F.M., Soraghan, J. (2007). A new multistage lattice vector quantization with adaptive subband thresholding for image compression. *EURASIP Journal on Advances in Signal Processing*, 2007: 1-11. <https://doi.org/10.1155/2007/92928>
- [26] De Albuquerque, M.P., Esquef, I.A., Mello, A.G. (2004). Image thresholding using Tsallis entropy. *Pattern Recognition Letters*, 25(9): 1059-1065. <https://doi.org/10.1016/j.patrec.2004.03.003>
- [27] Kumari, G.V., Rao, G.S., Rao, B.P. (2018). New bacteria foraging and particle swarm hybrid algorithm for medical image compression. *Image Analysis & Stereology*, 37(3): 249-275. <https://doi.org/10.5566/ias.1865>
- [28] Ahilan, A., Manogaran, G., Raja, C., Kadry, S., Kumar, S.N., Kumar, C.A., Murugan, N.S. (2019). Segmentation by fractional order Darwinian particle swarm optimization based multilevel thresholding and improved lossless prediction based compression algorithm for medical images. *IEEE Access*, 7: 89570-89580. <https://doi.org/10.1109/ACCESS.2019.2891632>
- [29] Hoang, T.M., Zhou, J., Fan, Y. (2020). Image compression with encoder-decoder matched semantic segmentation. 2020 IEEE/CVF Conference on Computer Vision and Pattern Recognition Workshops (CVPRW), pp. 619-623. <https://doi.org/10.1109/CVPRW50498.2020.00088>
- [30] Sarkar, S., Das, S. (2013). Multilevel image thresholding based on 2D histogram and maximum Tsallis entropy—a differential evolution approach. *IEEE Transactions on Image Processing*, 22(12): 4788-4797. <https://doi.org/10.1109/TIP.2013.2277832>
- [31] Farnad, B., Jafarian, A., Baleanu, D. (2018). A new hybrid algorithm for continuous optimization problem. *Applied Mathematical Modelling*, 55: 652-673. <https://doi.org/10.1016/j.apm.2017.10.001>